Int. Journ. of Unconventional Computing, Vol. 0, pp. 1–21
Reprints available directly from the publisher
Photocopying permitted by license only

Robustness of the Critical Behaviour in the Stochastic Greenberg-Hastings Cellular Automaton Model*

HUGUES BERRY[1] AND NAZIM FATÈS[2]

[1]*INRIA Grenoble-Rhone-Alpes, Beagle team, Campus de La Doua, 69 603 Villeurbanne, France*
E-mail: hugues.berry@inria.fr

[2]*INRIA Nancy-Grand Est, LORIA, MaIA team, Campus Scientifique, B.P. 239, 54 506 Vandoeuvre-lès-Nancy, France*
E-mail: nazim.fates@loria.fr

Received: July 30, 2010. Accepted: January 6, 2011.

We study a stochastic version of the Greenberg-Hastings cellular automaton, a simple model of wave propagation in reaction-diffusion media. Despite its apparent simplicity, its global dynamics displays various complex behaviours. Here, we investigate the influence of temporary or definitive failures of the cells of the grid. We show that a continuous decrease of the probability of excitation of cells triggers a drastic change of behaviour, driving the system from an "active" to an "extinct" steady state. Simulations show that this phenomenon is a nonequilibrium phase transition that belongs to directed percolation universality class. Observations show an amazing robustness of the critical behaviour with regard to topological perturbations: not only is the phase transition occurrence preserved, but its universality class remains directed percolation. We also demonstrate that the position of the critical threshold can be easily predicted as it decreases linearly with the inverse of the average number of neighbours per cell.

Keywords: Stochastic cellular automata, reaction-diffusion, non-equilibrium phase transitions, robustness

*This research was supported by French National Institute for Computer Science and Control (INRIA), grant ARC AMYBIA.

1 INTRODUCTION

Reaction-diffusion systems are a class of dynamical systems that have been used to model a large class of natural phenomena. In 1952, Turing proposed to couple reactions and diffusion of some imaginary chemical components, the *morphogens*, to explain how structured patterns could appear in initially symmetric organisms [21]. Since then, reaction-diffusion systems were used in the description of phenomena in various fields, such as mollusk shell pigmentation (*e.g.*, [16]), heart modelling (*e.g.*, [17]), etc.

This article presents a discrete and stochastic version of reaction-diffusion systems. The model we study is a stochastic variation of the classical Greenberg-Hastings cellular automaton (GHCA) [13]. The GHCA is arguably the simplest discrete model to mimic reaction-diffusion waves. Broadly speaking, this model considers that a CA cell can jump to an excited state when at least one of its neighbours on the CA lattice is itself excited (local transmission). Once excited, a cell de-excites at the next time step and then has to wait for a certain period of time before it can be excited again (refractory period). These two elements, local transmission plus refractory period, are the basic ingredients that allow the GHCA to mimic propagating wave fronts.

In spite of its apparent simplicity, this model displays complex behaviours. In particular, when the transmission probability varies, the GHCA undergoes a critical phase transition from an active (alive) into an extinct (dead) phase [10, 9]. Moreover, the properties of the model are especially suitable for technology-oriented applications. For instance, we have recently proposed a bio-inspired system based on GHCA, to achieve decentralised and robust gathering of mobile agents scattered on a surface [9].

As usual with such models, the GHCA has mainly been studied using a homogeneous and regular lattice. To our knowledge, the only exception is a recent study of its dynamics on scale-free networks [4]. However, in the context of massively distributed computing, one also needs to consider unreliable elements and defect-based noise. Our goal here is thus to broaden the knowledge on stochastic reaction-diffusion media by investigating how such systems behave when various types of noise are introduced. Therefore we modify the GHCA model to take into account the heterogeneity that could exist in an imperfect environment. We consider two types of heterogeneities: *temporary failures*: a cell might not receive an excitation from its neighbours, *definitive failures*: we consider two types of definitive failures; (a) a defective cell never gets excited, this is equivalent to putting "holes" in the grid; (b) links between two neighbouring cells might be broken.

We show that this perturbation may change qualitatively the evolution of the system. More precisely, varying the probability to receive an excitation triggers a phase transition between an "active" and an "extinct" macroscopic state. Our experiments show that this phase transition belongs to the universality class of directed percolation. We use this information to measure the

critical threshold with precision. We show that the position of this threshold highly depends on the topological properties of the grid. From these first observations, we propose to establish a law which states that the value of the critical probability is inversely proportional to the size of neighbourhood.

2 MODEL AND METHODS

2.1 The Model

The system evolves according to stochastic cellular automata dynamics. Space is modelled by a regular lattice $\mathcal{L} = \{1, \ldots, X\} \times \{1, \ldots, Y\}$ in which each cell is denoted by $c = (c_x, c_y) \in \mathcal{L}$. The set of possible states for each cell is $\{0, \ldots, M\}$: the state 0 is the *neutral* state, the state M is the *excited* state, the states 1 to $M-1$ are the *refractory states*. Each cell c is associated with a set of cells, $\mathcal{N}_c$, its *neighbourhood*, which captures the locality of the influences between cells (see below). We denote by σ_c^t the state of a cell c at time t.

We call neutral, excited, or refractory, a cell of a given configuration that is in the neutral, excited, or refractory state, respectively. The evolution of a cell is represented on Fig. 1 ; it is described as follows:

- A neutral cell stays neutral unless it has (at least) one excited neighbour. It then becomes excited with probability p_{T}, the *transmission rate*.
- An excited cell becomes refractory ($M-1$) in one step.
- A refractory cell decrements its state until it becomes neutral.

Formally, let E_c^t be the number of excited cells in $\mathcal{N}_c$ at time t: $E_c^t = \mathrm{card}\{c' \in \mathcal{N}_c \,|\, \sigma_{c'}^t = M\}$. The local rule governing the evolution of each cell is a stochastic version of the classical Greenberg-Hastings model [13]:

$$\forall t, \forall c, \quad \sigma_c^{t+1} = \begin{cases} M & \text{if } \sigma_c^t = 0 \text{ and } E_c^t > 0 \text{ with probability } p_{\mathrm{T}} \\ \sigma_c^t - 1 & \text{if } \sigma_c^t \in \{1, \ldots, M\} \\ 0 & \text{otherwise} \end{cases} \tag{1}$$

In this paper, we use the following neighbourhood types:

- 4-nearest-neighbours (North, East, South, West adjacent cells).
- 8-nearest-neighbours (adjacent + diagonal cells).
- 6-nearest-neighbours (adjacent cells on a hexagonal grid).

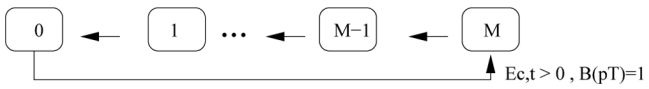

FIGURE 1
Transition rule of the reaction-diffusion system

- The circular neighbourhood. It was introduced by Markus and Hess to model isotropic reaction-diffusion systems [18]. To obtain this neighbourhood, we start from a square 2D lattice, then we transform the integer coordinate of the cells into real coordinates by adding a random component uniformly chosen in $[0, 1]$. The neighbourhood of radius R of cell c is the set of cells with an Euclidean distance to c less than R (using the real coordinates of cell).

These topologies are associated with the codes V4, M8, H6, CIr, respectively, where r is the radius of the circular neighbourhood. Figure 2 illustrates the importance of the topology on the aspect of the emitted waves, in the case of perfect transmission (*i.e.*, $p_T = 1$). In the following, we study how the topology affects the asymptotic behaviour of the system.

As already introduced above, we use two methods to model definitive failures in the system:

1. A first method consists in introducing holes at random in the lattice. In this case, before starting the simulation, we consider each CA cell in turn independently, and with probability HR (for Hole Rate), we remove this cell from the lattice (this is equivalent to setting $\sigma_c^t = 0$ for all t for this cell).
2. The other method consists in removing neighbourhood links between cells. To this aim, we consider for each cell all the other cells in its regular

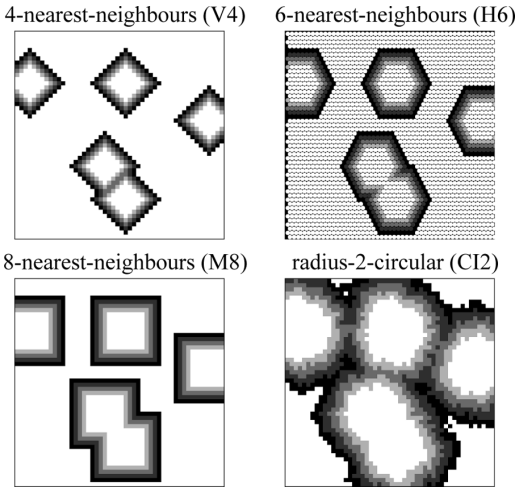

FIGURE 2
Influence of the topology on the reaction-diffusion waves with perfect transmission ($p_T = 1$). We take $M = 4$, simulation time $t = 8$ and start from the same initial condition with five excited cells. The color of the cells represent their state: white is neutral (0), black is excited (M), gray levels represent the refractory states (1 to M-1).

neighbourhood and remove the link to this cell with probability MLR (for Missing Link Rate). Links are removed definitively, and before simulation starts.

2.2 Phase Transitions

To evaluate the effects of local temporary failures (noise) on the *macroscopic* behaviour of the model, we monitored the time evolution of a macroscopic quantity, the average density of excited cells $d_M(t)$, that is, the total number of cells in state M at time t divided by the total number of cells. Figure 3A shows typical evolutions of $d_M(t)$ for different failure levels. When excitation probability p_T is high (*e.g.*, $p_T = 0.47$ in Fig. 3A), the system reaches a steady-state where d_M oscillates around a fixed value. In this steady state, excitation waves fluctuate in space and time, but their overall number is rather stable. This state can thus be referred to as the *active* steady-state. Now, when temporary failures are too frequent (*i.e.*, for low values of p_T), the density of excited cells rapidly decreases to 0 (*e.g.*, $p_T = 0.45$ in Fig. 3A). The system reaches an *extinct* state, where all cells are neutral and where the activity is definitively washed out.

Plotted in log-log coordinates (Fig. 3B), the convergence to the active steady state corresponds to an upward curvature of the density while convergence to the extinct state is accompanied by a down-ward curvature (exponential decay). As shown in this figure, a very small change in the value of p_T may have huge long-term effects as it can decide which steady

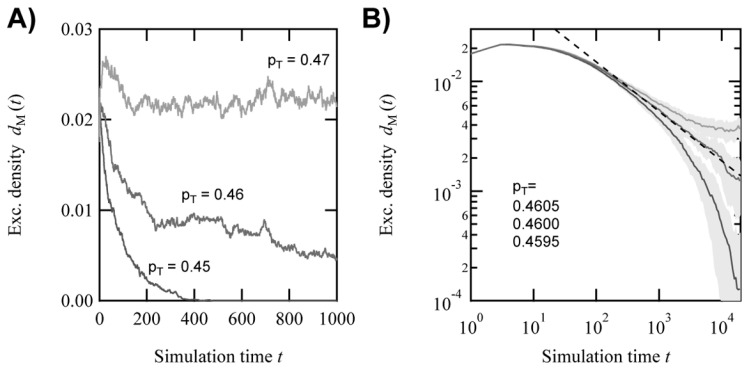

FIGURE 3
Evolution of the density of excited cells $d_M(t)$. (A) Single run with three values of the transmission rate: sub-critical $p_T = 0.45$ (purple), critical $p_T = 0.46$ (red), supra-critical $p_T = 0.47$ (green). (B) Log-log plot of the average of 30 runs for, from bottom to top (full lines): $p_T = 0.4595$ (purple), 0.4600 (red) and 0.4605 (green). The grayed zones around each curve indicate the standard deviation from the mean. The dashed line indicates a decay compatible with the behavior expected for 2D directed percolation: $d_M(t) \propto t^{-0.451}$. Settings: $L = 400$ (left) or 800 (right); 4-nearest-neighbours topology and $M = 4$.

state, whether extinct or active, is reached. This indicates the presence of a phase transition around a *critical threshold* $p_{\mathrm{T_c}}$, that separates the p_{T} values leading to the active state from those leading to the extinct state.

To analyse such a phase transition, we use the tools developed during the last decades by statistical physicists. The study of critical phenomena (whether equilibrium or non-equilibrium) has grown to a major research field for physics and developed a mature range of concepts and theoretical tools to understand and quantify such phase transitions. Our main objective is to study the macroscopic dynamics of the GHCA close to the phase transition, in particular when topological noise is added to the system. We now briefly present the concepts related to phase transitions that will be used thereafter in the paper.

Statistical physics tells us that near the critical threshold, the laws governing the phase transition are power laws [14]. Informally, we can say that the emergence of these power laws is a consequence of a spatial organisation of the system with scale-invariant patterns. For instance in our case, one expects $d_M(t) \sim t^{-\delta}$ at the critical threshold $p_{\mathrm{T}} = p_{\mathrm{T_c}}$ which means that, in log-log plots as in Fig. 3B, the critical threshold should produce a straight line. It is also a well-established fact that different systems may display identical critical exponent values [14], which means these systems share identical fundamental properties. Systems sharing the same critical exponent values are said to belong to the same *universality class*.

The universality class of directed percolation was observed in many discrete or continuous spatially-extended systems. One of the first observations of directed percolation was performed on the Domany-Kinzel cellular automaton [15, 6]. Directed percolation was also observed in simple cellular automata such as the Game of Life [3, 8], or 1D Elementary Cellular Automata [7, 20]. In the case of the GHCA, we have previously found evidence that it belongs to the universality class of directed percolation, *i.e.*, $\delta = 0.451$ [9].

Note that statistical physics predicts that δ is a universal quantity, that is, its value depends on the dimension of the lattice but not on details of the model. By contrast, the location of the critical threshold $p_{\mathrm{T_c}}$ is not universal and depends on details of the model, such as the number of states, the lattice topology, etc. Therefore it must be evaluated by other means. Finding the critical threshold is particularly important if we use our reaction-diffusion medium as a computing device. Indeed, the main properties of our system, the average wave length for instance, highly depend on the fact that the excitations will "percolate" through the medium or not. We now present how to measure the position of the critical threshold, depending on the quantity of defects in the lattice, and how to predict this position with mean-field techniques.

2.3 Experimental protocol

Measuring the universal exponents and the critical probability is a delicate task that requires a rigorous protocol. In this paper, we choose to measure the position of the critical probability by spotting changes of convexity in

log-log curves (see [14, 19, 7]). In order to study a phase transition, one needs to define an order parameter, that is, a quantity that describes at the macroscopic level the state of the system, and a control parameter, that is, a parameter for which a minor variation may induce a qualitative change of the order parameter. From the inspection of Fig. 3, a natural choice consists of the density of excited cells $d_M(t)$ and the transmission probability p_{T} as order and control parameters, respectively.

There are various methods to determine the suitable values of the simulation parameters such as the size of the grid L, the time of observation T and the number of samples S for extracting average values. They generally involve a trade-off between two contradictory objectives: (a) the values of L, T and S should be as large as possible to allow for the best approximation of an infinite-size system ; (b) the computation time should be kept reasonable.

To fix these parameters, we first define a reference system: the topology is set to the 4-nearest-neighbours and the value of excitation level is $M = 4$. Our strategy consists in doubling the value of the grid size, setting $L \in \{100, 200, 400, 800\}$. For each value of L, we determine an upper and lower bound for the estimation of $p_{\mathrm{T_c}}$ by inspection of the convexities of the excited density $d_M(t)$ curves in log-log plots. We then progressively diminished this interval of uncertainty on $p_{\mathrm{T_c}}$ by using increasing values of L and, simultaneously, by increasing the value of T and S. Indeed, the closer to $p_{\mathrm{T_c}}$, the longer the simulation time needed to observe the concavity change of the curves. This phenomenon, called *the critical slowing down* is often the limiting factor for determining the precision on $p_{\mathrm{T_c}}$ (see *e.g.* [14]).

Using the above described methods, we refined the measures on $p_{\mathrm{T_c}}$ until its estimation interval size is of the order of 10^{-4}. Usually, using $L = 800$, $T = 20,000$ and $\mathrm{S} = 40$ runs was enough to reach such accuracy. However, whenever these settings were not sufficient to clearly spot the phase transition, we further increased the grid size to $L = 1200$.

3 ROBUSTNESS STUDIES

In this section, we describe a series of three experiments designed to test the robustness of the phase transition from the "active" to the "extinct" state. We first modify the value of the excitation level M. Then, we introduce topology effects (holes and missing links) in the grid. In all cases, we examine if the phase transition is still observed, and if yes, what is its universality class and how it is affected by the perturbations we introduced.

3.1 Robustness to variations of the excitation level

As a first step for the analysis of the robustness of the phase transition, we varied the excitation level M and examined how $p_{\mathrm{T_c}}$ is modified. Figure 4

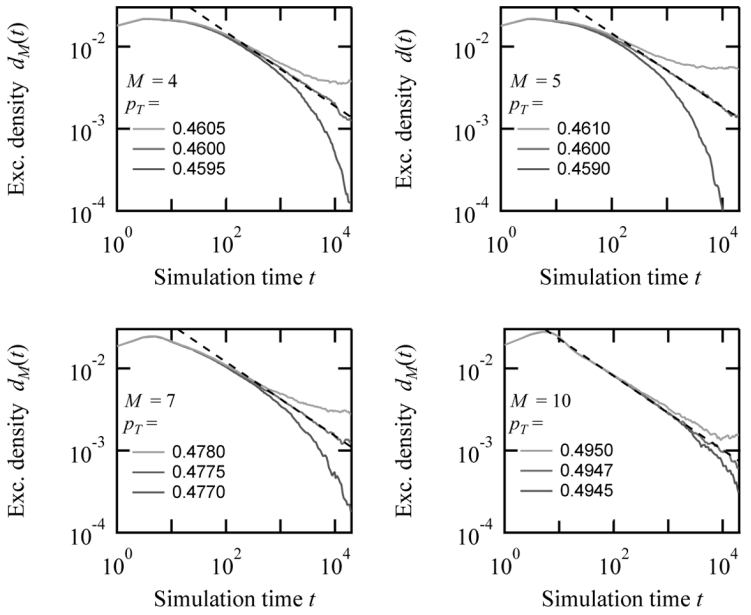

FIGURE 4
Robustness of the phase transition to changes of the excitation level M. Temporal decay of the density of excited cells $d_M(t)$ for different values of p_T around the critical value. The dotted line indicates a power law expected for directed percolation in 2D (*i.e.*, $d_M(t) \propto t^{-0.451}$). Curves are obtained with an average of 30 independent runs, a lattice size $L = 800$, 4-nearest-neighbours topology and periodic boundary conditions.

shows the decay of the density of excited cells $d_M(t)$ during simulations carried out with 4-nearest-neighbours and M ranging from 4 to 10. First of all, we observed that the critical exponent δ was in all cases in agreeement with directed percolation, that is, the values determined from the simulations were statistically compatible with those for directed percolation.

Beyond the data presented in this figure, we evaluated δ for values of M ranging from 2 to 10 and various topologies (see our website[1]). The resulting estimates of $p_{\mathrm{T_c}}$ are plotted in Fig. 5. We noticed that $p_{\mathrm{T_c}}$ slightly increases with M (from 0.42 to 0.49 when M ranges from 2 to 10). At first sight, one may judge this variation moderate (less than 17%). It is an open question to determine if there is an asymptotic behaviour of the system for large values of M. From a practical point of view, an increase in M results in the emergence of longer waves, which implies that larger grids are required to measure the phase transition. As far as we could say, for all the values of M we tested, the observed phase transition was in a good agreement with directed percolation.

[1] see `http://webloria.loria.fr/~fates/Amybia/reacdiff.html`

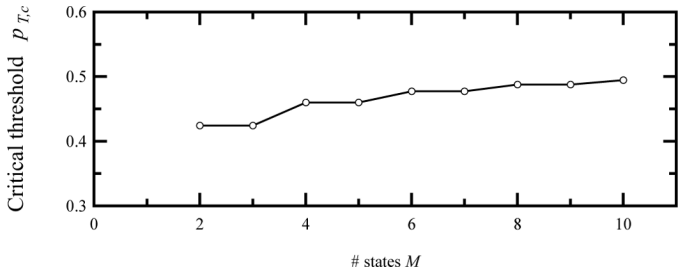

FIGURE 5
Critical values for the data reported above.

However, we reached a limitation for finding $p_{\mathrm{T_c}}$ experimentally for large values of M because of an increased amount of noise that appeared in the measures. The origin of this noise can be understood as follows. We first note that in the asymptotic case where M is infinite, a cell can be excited *only once* because the time to de-excite is infinite. This implies that the phase transition is expected to belong to the *dynamical percolation* [5] universality class. Hence a "naive" approach would expect that we observe a different critical exponents for the $M \to \infty$ case. If this were the case, the cluster of excited cells would be a percolation cluster at the (isotropic) percolation threshold, and thus, we expect to observe $p_{\mathrm{T_c}} = 0.5$ with 4-nearest-neighbours topology.

However, our estimations for large values of M yielded values somewhat larger than this asymptotic limit [22]. The noise observed can thus be interpreted as a progressive crossover from the directed to the dynamical percolation regime as M increases. In fact, at intermediate M values, the apparent universality class (hence the exponent values) is expected to change *during the simulation* [12]. This "tension" between two universality classes may explain why it is difficult to evaluate the critical threshold in an accurate and reliable way and why our our estimations at large M values are far less accurate than with smaller values.

We nevertheless noticed an interesting phenomenon: the values of the critical threshold seem to be identical by pairs, for $M = 2k$ and $M = 2k + 1$ and $k \geq 1$. Although we tested this property only for $M \leq 10$, we conjecture that it holds for every $M \geq 2$. More surprisingly, this property is not general: it was not observed for any other topology we tested. We leave the study of this even-odd invariance as an open question for future work.

3.2 Holes and missing links

We now evaluate the effects of failures: a cell might be defective and no longer respond to excitations. What happens in this case? How is the phase transition affected by the rate of defective cells? Intuitively, we imagine that the higher the rate of defects, the more difficult it will be for the active phase to maintain. The next experiments we present are intended to quantify this intuition.

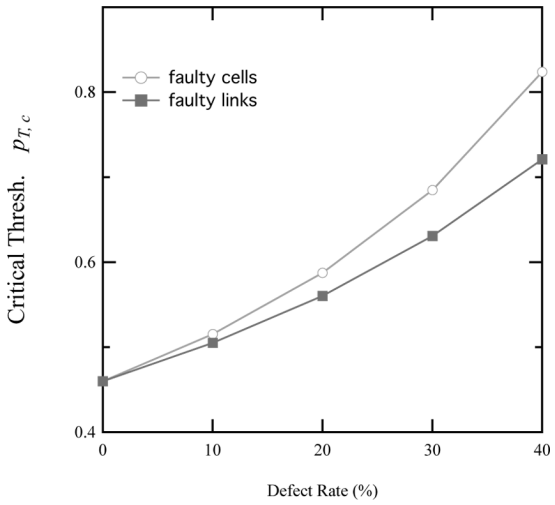

FIGURE 6
Evolution of the critical threshold $p_{\mathrm{T_c}}$ as a function of hole rate HR (empty circles) or missing link rate MLR (closed squares). The curves are obtained with S = 15 runs, $M = 4$, lattice size $L = 1200$, and with the 4-nearest-neighbours topology. Each run starts from a different initial condition with different defect positions.

The effect of these perturbations are shown on Fig. 6. To evaluate the effects of permanent failures on the phase transition, we varied the hole rate HR, and the missing link rate MLR, from 0 to 0.4 by increments of 0.1. As expected, the critical threshold increases with the defect rate. This can be easily understood since the removal of cells or the suppression of links between cells decreases the probability to transmit excitation across the lattice. As a consequence, the difficulty to transmit waves has to be "compensated" by an increase in the transmission probability, which explains the rise of $p_{\mathrm{T_c}}$.

3.3 A "blurring effect"

Surprisingly enough, we observed that as the defect rates increased, the critical threshold $p_{\mathrm{T_c}}$ became more difficult to determine. From a practical point of view, it was difficult to go beyond HR $= 0.40$ or MLR $= 0.40$. All happened as if the transition between the extinct and active regime was "blurred" by the increase of defects in the topology.

Simulation results for the cases where 40% of the cells or links are faulty are presented in Fig. 7. In both cases (faulty cells or faulty links), the phase transition is much more difficult to locate and estimations of the change in curvature are less precise. Even in these large-size simulations, sub- and supra-critical curves appear closer to a power law, *i.e.*, in log-log coordinates, these curves seem closer to linear rather than bending up or down, even far

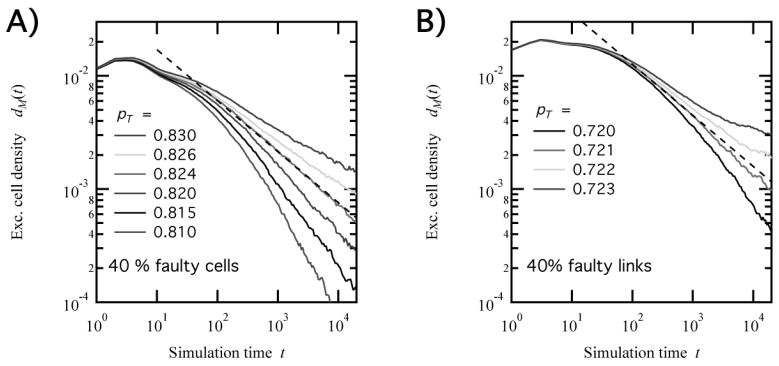

FIGURE 7
Robustness of the phase transition with defects in the lattice. 40% of the cells (*A*) or of the links (*B*) were destroyed. Other parameters as in Fig. 6.

from the threshold. It is thus more delicate to locate the critical threshold with a good precision.

To our knowledge, this is the first observation of such a phenomenon. We believe that the origin of this "blurring effect" is closely linked to the correlation length and self-scaling properties of the underlying graph. Indeed, as the faults rate increase, the simulations show large finite size effects, which appear as an increase in the noise or as premature extinctions of the waves. A very large number of simulations in the supra-critical regime fall into the extinct state. As a result, instead of curving up, curves obtained in supra-critical conditions seem to first curve up then down, for instance. To avoid these caveats, we had to increase increase the lattice size L.

Note that the underlying graph, *i.e.*, the graph built on the non-faulty site (or links), is an isotropic (bond or site) percolation cluster whose distance to the threshold is set by HR and MLR. As a consequence, as HR and MLR approach the critical value $1/2$ (for isotropic percolation), the dynamics of the system can be thought as a directed percolation system whose evolution is restricted to remain on an isotropic percolation cluster at the threshold. The study of the interplay of these percolation types is an interesting perspective of the present results. Note however that it is important to remark that this system radically differs from the systems constructed to study the crossover (or hybridisation) between isotropic and directed percolation [11].

In spite of these issues, long simulations allowed us to determine the values of the critical threshold and exponent δ. It is impressive to observe that for all the conditions we tested, δ remained compatible with directed percolation (see Fig. 7 and other simulations available on the web site[1]). Hence, albeit the precision is lower, these simulations show that the phase transition and the universality class are conserved in our model, even when close to half of the cells or links are destroyed.

3.4 Changing the topology

We first studied whether the nature of the boundaries (periodic, reflexive or free) could change the observed phenomenon. Our results (not shown) unambiguously showed that both the value of the critical threshold and the nature of the phase transition, that is, its universality class, was not modified by the boundary conditions in our simulations. Likewise, adding the cell under consideration in its own neighbourhood does not change the critical threshold nor the phase transition (the effect of the transition rule is unchanged as only the transition from 0 to M depends on the neighbourhood state).

We next examined how the different neighbourhoods (*i.e.*, different connection of the cells) affect the phase transition. Figure 8 and 9 shows determinations of critical threshold $p_{\mathrm{T_c}}$ for various topologies and $M = 4$. Clearly, we observed that the critical threshold varies greatly with the topology while the critical exponent δ remained constant. These simulations showed that, again, directed percolation seems to remain the universality class of the observed phase transition *whatever the topology*. Interestingly enough, the data of Fig. 9 suggests that there exists a correlation between the value of $p_{\mathrm{T_c}}$ and the size of neighbourhood. We investigate this correlation in the next section.

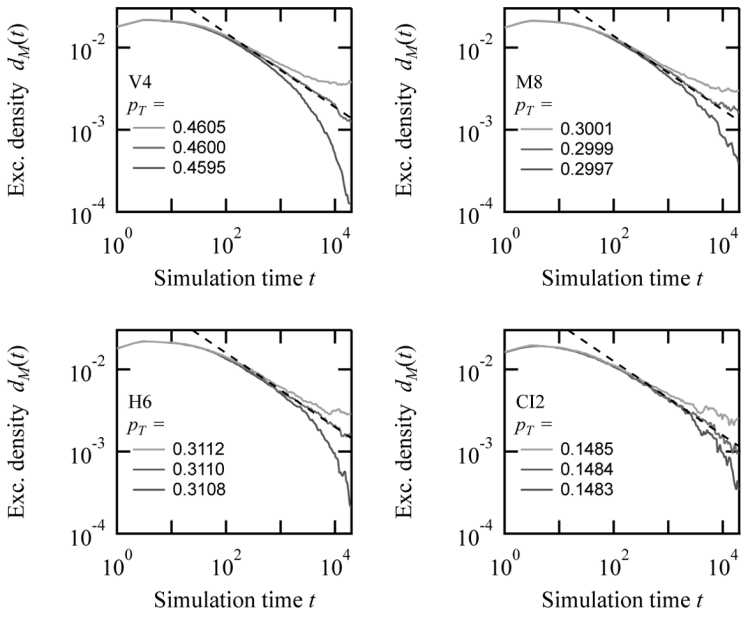

FIGURE 8
Robustness of the phase transition to topological changes (with $M = 4$). Decay of the instantaneous densities of excited cells $d_M(t)$ with time for various topologies and p_T values. See text for the topology code convention. Other parameters are like in figure 4.

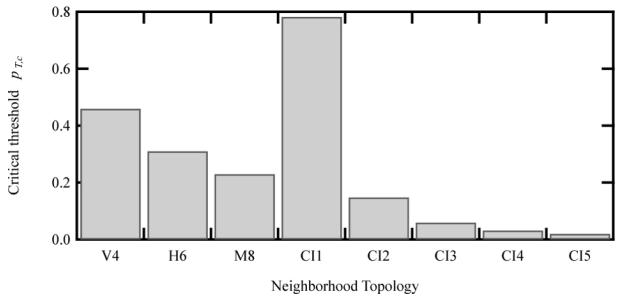

FIGURE 9
Critical values for a regular grid and different neighbourhoods (see above)

4 THE INVERSE PROPORTIONALITY LAW

The previous section confirmed the robustness of the directed percolation phase transition to changes of the model. We now focus on the value of the critical threshold. We noticed that in general the higher the defects, the higher the critical probability. But can this effect be estimated quantitatively? In this section we propose to establish a law of inverse proportionality: the value of $p_{\mathrm{T_c}}$ is inversely proportional to the number of neighbours in the neighbourhood. First we give a theoretical analysis supporting this hypothesis, second we test the hypothesis on the restricted set of the previous experiments.

4.1 Mean-field approximation

We present here an approximation of the behaviour of the model Eq. 1 using mean-field arguments. More precisely we write down differential equations based on conservation principles and assume that spatial fluctuations of cell densities are negligible.

Let $d_i(t)$ be the density of cells in state i at time t, *i.e.*, the number of cells in state i at time t over the total number of cells of the lattice. We focus on a continuous-time equivalent of the GHCA model, hypothesising that this continuous-time assumptions does not drastically modify the expected behaviours. Under this assumption, conservation principles on the basis of the transition rules (Eq. 1) can be expressed as a system of ordinary differential equations:

$$\left\{\begin{array}{rcl} \dot{d_0}(t) & = & d_1(t) - p_T d_0(t)\pi_0(t) \\ \dot{d_j}(t) & = & d_{j+1}(t) - d_j(t); \quad \text{for } j \in \{1,\ldots,M-1\} \\ \dot{d_M}(t) & = & p_T d_0(t)\pi_0(t) - d_M(t) \end{array}\right. \tag{2}$$

where $\pi_0(t) = \mathrm{prob}\left(E_c^t \geq 1 | \sigma_c^t = 0\right)$ is the conditional probability that there is at least one cell in excited state M in the neighbourhood of a cell c, given that c is in state 0. As this is equivalent to *not* having all the neighbours

in a non-excited state, by considering that the states of the neighbours are independent, we have:

$$\pi_0(t) = 1 - \prod_{c' \in \mathcal{N}_c} \left[1 - \text{prob}\left(\sigma_{c'}^t = M | \sigma_c^t = 0\right)\right].$$

We now make the simplifying assumption that the spatial fluctuations of prob $\left(\sigma_c^t = M\right)$ can be neglected and consider that this value is identical at each point of the lattice (spatially homogeneous). With these assumptions, the latter probability is simply given by the cell density, prob $\left(\sigma_c^t = M\right) = d_M(t)$ and one finally obtains: $\pi_0(t) = 1 - (1 - d_M(t))^N$ where N is the average size of the neighbourhood, *i.e.*, $N = \langle \text{card}\,\{\mathcal{N}_c\}\rangle$, and brackets $\langle . \rangle$ denote averaging over the cells.

Eq. 2 then becomes:

$$\left\{ \begin{array}{rcl} \dot{d_0}(t) & = & d_1(t) - p_T d_0(t)\left[1 - (1 - d_m(t))^N\right] \\ \dot{d_j}(t) & = & d_{j+1}(t) - d_j(t); \quad \text{for } j \in \{1, \ldots, M-1\} \\ \dot{d_M}(t) & = & p_T d_0(t)\left[1 - (1 - d_m(t))^N\right] - d_M(t) \end{array} \right. \tag{3}$$

We then look for the steady-states d_i^* of Eq. 3. They are given by $\dot{d}_i(t) = 0$; for $i \in \{0, \ldots, M\}$, *i.e.*, by setting the left-hand-side members of Eq. 3 to zero, then solving for the densities. After some easy manipulations, one finds that the steady-state density of excited cells, d_M^* is given by

$$d_M^* - p_T\left(1 - M d_M^*\right)\left[1 - \left(1 - d_M^*\right)^N\right] = 0 \tag{4}$$

The other steady-state densities can be deduced from d_M^* by

$$d_i^* = d_M^*; \ \forall i \in \{1, \ldots, M-1\}$$

and

$$d_0^* = 1 - M d_M^*.$$

As a result, we obtain the first trivial steady state $d_M^* = 0$, for all p_T. This fixed point corresponds to a configuration where all cells are in the neutral state $\sigma_c = 0$. This state, once reached, cannot be escaped, *i.e.*, it corresponds to the death of the system. This state is in fact the "extinct" state observed in our GHCA simulations reported above. Figure 10 shows a numerical bifurcation analysis of the system of Eq. 3 with the extinct state in red (horizontal line). This figure evidences the existence of a second steady-state (green in the figure). This steady-state varies with p_T and corresponds to strictly positive

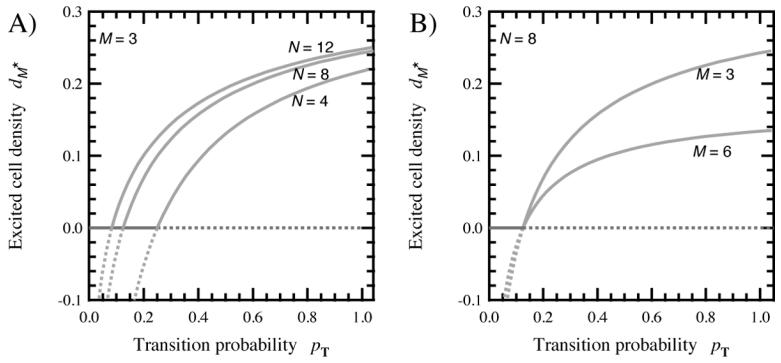

FIGURE 10
Bifurcation analysis of the Mean-Field equations 3. Steady-state densities of excited cells d_M^* as a function of p_T with $M = 3$ states and $N = 4$, 8 or 12, from bottom to top (A) or $N = 8$ and $M = 3$ or 6 (B). Stable fixed point are depicted with full lines, and unstable ones with dotted lines.

values for d_M^*, *i.e.*, to a state in which part of the cells are in the excited or a refractory state. This second steady-state corresponds to the active steady-state of our GHCA simulations above.

Having determined these two states is not enough for showing that a phase transition occurs. The second step is to analyse the stability of the points. On Fig. 10, stability and instability are indicated by full or dotted lines, respectively. We observe that the extinct state is stable up to the intersection point between both steady-states. At the intersection, the two steady-state exchange stability: the active one becomes stable, while the extinct ones becomes unstable. Technically, the intersection point is called a transcritical bifurcation and it predicts the occurrence of a qualitative change of behaviour of the system. More precisely, for $p_T < p_{\mathrm{T_c}}$ one expects the system to reach at long times the extinct (dead) state, where all cells are neutral, while an active state is expected as soon as $p_T > p_{\mathrm{T_c}}$. A critical regime is thus expected at the critical threshold $p_T = p_{\mathrm{T_c}}$.

We can now obtain an evaluation of $p_{\mathrm{T_c}}$ as a function of M and of the topology. We use a series expansion at order 1 of the left-hand-side term in Eq. 4 for $d_M^* \to 0$ (higher orders yield similar results):

$$d_M^* - p_T \left(1 - M d_M^*\right) \left[1 - \left(1 - d_M^*\right)^N\right] \approx (1 - P_T N)\, d_M^* + O\left({d_M^*}^2\right).$$

Eq. 4 can thus be approximated by

$$(1 - p_T N)\, d_M^* = 0.$$

p_{Tc} is the value of p_T that satisfies the latter equation. This yields the following approximation:

$$p_{\mathrm{Tc}} = \frac{1}{N} \tag{5}$$

Eq. 5 indicates that p_{Tc} is expected to depend on the average neighbourhood size N but not on the number of cell states M. This is confirmed by the numerical studies of Fig. 10. But this equation is more precise, as it predicts that p_{Tc} is expected to scale as the inverse of N.

4.2 Experimental testing of the law

We now test the validity of the mean-field prediction: does p_{Tc} vary proportionally to the inverse of the neighbourhood size N?

Figure 11 displays the critical thresholds for all the simulation we have run (various topologies, various defect rates, various M values) as a function of the corresponding neighbourhood size N. The critical thresholds for all the topology tested previously (see Fig. 9) are plotted as a function of their neighbourhood size N (open squares in Fig. 11). We also add on this figure

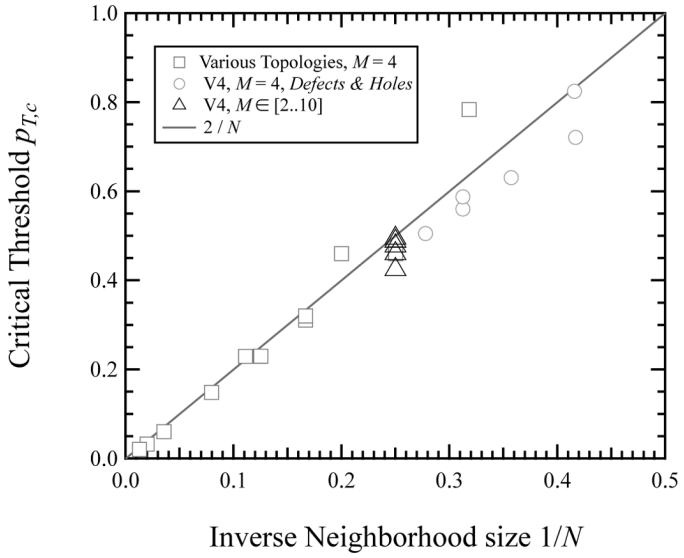

FIGURE 11
Illustration of the proportionality law between p_{Tc} and $1/N$, where N is the average number of neighbours. Square marks correspond to different topologies (see Fig. 9). Green circles correspond to $M = 4$ and V4 topology modified by various rates of defects (see Sec. 3.2 and Fig. 6). Black triangles correspond V4 topology with M varying from bottom to top from 2 to 10 (see Fig. 5). The red line shows the curve $p_{\mathrm{Tc}} = 2/N$.

(open circles) the values obtained with a 4-nearest-neighbours topology where various defect rates are added (see Sec. 3.2 above).

Strikingly, the points align on a straight line and fitting over the data we obtained yields:

$$p_{\mathrm{T_c}} \approx 2/N. \tag{6}$$

Therefore, our mean-field approach nicely predicts the observed N^{-1} dependency of the critical threshold. It thus shows that the important quantity to determine the value of the critical threshold is the average number of neighbours per cell and not the detail of the topology or its homogeneity. This is illustrated by the fact that the data for both perfect (*i.e.*, defectless) topologies and those with various degree of defects can be described by the same law.

The mean-field approach however fails to predict several quantitative features of the simulations. First of all, note that the value of the prefactor in the scaling law Eq. 6 was predicted to be 1, whereas the simulations rather indicate a value of 2. More intriguingly, the mean field approach predicts that $p_{\mathrm{T_c}}$ does not depend on the number of cell states M. Yet, we have already seen above that this is not observed in our simulations: $p_{\mathrm{T_c}}$ increases slightly with M. However, this increase is moderate enough that the observed values are still roughly in agreement with the N^{-1} scaling, as seen in Fig. 11 (triangles).

In any case, these discrepancies can be related to the assumptions made in the mean field approach, in particular that the spatial (or cell-to-cell) fluctuations in the number of active neighbours are negligible. Actually, as M increases, the time spent by an excited cell in the refractory state (before recovering to the neutral one) increases. This would mean that local fluctuations of the number of excited neighbours will take much longer to disappear when M is large and explains the observed dependency of $p_{\mathrm{T_c}}$ on M.

5 DISCUSSION

The observations reported in this paper confirmed the great robustness of the directed percolation universality class. Although this statement is not new, it is to our knowledge the first time that this robustness was confronted against such a large number of variations: excitation level, holes in the grid, missing links, change of topology.

The experimental protocol allowed us to measure the critical threshold with a good precision (10^{-4}). However, when the rate of topological defects was too high, besides the critical slowing down, a new limiting factor appeared. It seems that as the regularity of the topology was destroyed, the distinction between the active and extinct phase was more difficult to spot. To our knowledge, little is known yet about this "blurring effect" and it is an open question to understand the origin of this phenomenon. Moreover, we reported

on an even-odd invariance of the critical threshold with M with the four-nearest-neighbours topology ; here too, theoretical explanations would be welcome.

The directed percolation conjecture It is a challenging question to explain this robustness with analytical arguments. The most common hypothesis that has been invoked to explain the impressive robustness of the universality class of directed percolation is due to Jansen and Grassberger (see [14] for an overview of this topic). In short, this conjecture states that a system should belong to the directed percolation universality class if it verifies the four following conditions:

(a) The model displays a continuous phase transition from a fluctuating active phase to a *unique* absorbing state.

(b) It is possible to characterise the phase transition by a positive one-component order parameter.

(c) The dynamics of the model is defined by short-range process, and

(d) there exists no additional symmetries or quenched randomness (*i.e.*, small frozen topological modifications).

These conditions are *sufficient* conditions for observing directed percolation. Our experiments suggest that the second part of condition (d) which regard quenched randomness does not apply for our system: in all cases directed percolation was observed, although it was also noted that too much topological defects made the measurement of the phase transition more delicate ("the blurring effect"). It should also be noted that the condition (a) is an *a posteriori* condition: it is first necessary to observe that there is a phase transition *then* we can deduce that its universality class is directed percolation. The question to know *what triggers* a phase transition is left open.

The observations reported in this paper may also provide first hints to clarify these questions: the position of the phase transition is strongly related to the size of the neighbourhood of the model. Although, this statement was observed on a restricted set of observation, it may well apply to a larger class of systems. To explore to which extent this inverse proportionality law is general opens a path for future work.

So far we examined the behaviour of our reaction-diffusion model for its own sake. We now briefly discuss how this simplified model of excitable media can be related to the issue of non-conventional computing.

Computing with colliding waves The idea to use excitable media as a novel means of computation dates from the early times of computer science: Turing realised that a set of cells embedded with simple reaction-diffusion local rules could develop into stable patterns [21]. However, interpreting these patterns in terms of computations was studied only recently, most remarkably by

Adamatzky and his coworkers [1]. Among the diverse techniques presented, collision-based computation consists of implementing logical gates by building appropriate circuits and coding bits as the presence or absence of waves. The authors show that a three-state logic can be derived from this coding and that it is possible to use this logic to run decentralised algorithms, most of them in the field of image processing.

Can this be transposed to noisy media? A specific study would be needed to answer this question but it is seems clear that a straightforward transposition of collision-based computing in a noisy medium is *not* possible. Indeed, the existence of delays in the propagation of wave would result in their collisions to be synchronised, which would possibly perturb the outcome of a computation. So we ask how to build a reaction-diffusion computing device which would compute even in the presence of noise. One possible solution could be to include source/sink sites in the networks that could locally delay or desynchronise wave propagation. Further works will be necessary to tackle this issue.

Computing on irregular networks In another context, Assis and Copelli proposed to use the stochastic Greenberg-Hastings cellular automaton on irregular networks to explain how biological organisms can exhibit a great range of input-output response to a stimulation [2]. Their model uses the probability that a cell gets spontaneously excited and they observe the density of excited cells. They show that the best setting of the system in terms of dynamic range response is precisely near the phase transition that separates the extinct and active state. The authors argue that this mechanism could be for instance used in the design of artificial sensors. They also reported that these properties are slightly altered when the network adopts an irregular structure, e.g. a scale free topology [4].

In our case, the networks used to test the behaviour against definitive failures (in particular in the case of missing links) are a first step from regular to irregular networks, but they remain rather close to regular. Preliminary studies with more irregular topologies (in particular rewiring links to randomly chosen nodes, in the spirit of Watts-Strogatz small-world networks [23]) did not show drastically different behaviours. Future work will be needed to investigate this aspect, though.

In this context, knowing the position of the critical threshold as a function of the topology is an important issue, especially if the cells of such a sensor would progressively die out. More generally, how could one predict the evolution of excitable media whose components are progressively altered?

Last, if we are given a network which structure is unknown, can we compute some topological information on this network by observing if a phase transition occurs? Answering this question requires a reversal of the viewpoint of the article. We so far adopted the physicist viewpoint by measuring how

the topology influenced the transition between two qualitative behaviours of the automaton. Conversely, we note that we could take a given network of cells and progressively decrease the probability of transmission. The moment where the system reaches the extinct state could give us the average connectivity of the cells for instance. Such a computation would not only have the advantage to be fully distributed and simple to implement, it would also be a promising path for the design of novel computing devices.

ACKNOWLEDGEMENTS

The authors express their acknowledgements to Nikolaos Vlassopoulos for his careful reading of the manuscript. Simulations were made with the *FiatLux* CA simulator (see http://www.loria.fr/∼fates/).

REFERENCES

[1] Andy Adamatky, Ben De Lacy Costello, and Testsuya Asai. (2005). *Reaction-Diffusion Computers*. Elsevier.

[2] Vladimir R. V. Assis and Mauro Copelli. (2008). Dynamic range of hypercubic stochastic excitable media. *Physical Review E*, 77(1):011923.

[3] Hendrik J. Blok and Birger Bergersen. (1999). Synchronous versus asynchronous updating in the "game of life". *Physical Review E*, 59:3876–9.

[4] M. Copelli and P.R.A. Campos. (2007). Excitable scale free networks. *European Physics Journal B*, 56(3):271–278.

[5] Stephan Dammer and Haye Hinrichsen. (2004). Spreading with immunization in high dimensions. *Journal of Statistical Mechanics: Theory and Experiment*, 2004(07):P07011.

[6] Eytan Domany and Wolfgang Kinzel. (1984). Equivalence of cellular automata to Ising models and directed percolation. *Physical Review Letters*, 53:311–314.

[7] Nazim Fatès. (2009). Asynchronism induces second order phase transitions in elementary cellular automata. *Journal of Cellular Automata*, 4(1):21–38.

[8] Nazim Fatès. (2010). *Game of Life Celluar Automata*, chapter Does *Life* Resist Asynchrony?, pages 257–274. Springer.

[9] Nazim Fatès. (2010). Solving the decentralised gathering problem with a reaction-diffusion-chemotaxis scheme - social amoebae as a source of inspiration. *Swarm Intellligence*, 4(2):91–115.

[10] Robert Fisch, Janko Gravner, and David Griffeath. (1993). Metastability in the Greenberg-Hastings model. *The Annals of Applied Probability*, 3(4):935–967.

[11] Erwin Frey, Uwe Claus Täuber, and Franz Schwabl. (Jun 1994). Crossover from isotropic to directed percolation. *Physical Review E*, 49(6):5058–5072.

[12] Peter Grassberger, Hugues Chaté, and Guillaume Rousseau. (1997). Spreading in media with long-time memory. *Physical Review E*, 55(3):2488–2495.

[13] J. M. Greenberg, B. D. Hassard, and S. P. Hastings. (1978). Pattern formation and periodic structures in systems modeled by reaction-diffusion equations. *Bulletin of the American Methematical Society*, 84(6):1296–1327.

[14] Haye Hinrichsen. (2000). Nonequilibrium critical phenomena and phase transitions into absorbing states. *Advances in Physics*, 49:815–958.

[15] Wolfgang Kinzel. (1983). Directed percolation. In R. Zallen G. Deutscher and J. Adler, editors, *Percolation Structures and Processes*, page 425. Adam Hilger Pub. Co., Bristol.

[16] Ingo Kusch and Mario Markus. (1996). Mollusc shell pigmentation: Cellular automaton simulations and evidence for undecidability. *Journal of Theoretical Biology*, 178(3):333 – 340.

[17] Danuta Makowiec. (2008). Cellular automata model of cardiac pacemaker. *Acta Physica Polonica B*, 39(5):1067–1085.

[18] Mario Markus and Benno Hess. (1990). Isotropic cellular automaton for modelling excitable media. *Nature*, 347:56 – 58.

[19] Géza Ódor. (2004). Universality classes in nonequilibrium systems. *Reviews of modern physics*, 76.

[20] Jean-Baptiste Rouquier and Michel Morvan. (2009). Coalescing cellular automata: Synchronization by common random source for asynchronous updating. *Journal of Cellular Automata*, 4:55–78.

[21] Alan M. Turing. (1952). The chemical basis of morphogenesis. *Philosophical Transactions of the Royal Society of London*, B 237:37–72.

[22] Nikolaos Vlassopoulos, Nazim Fatès, Hugues Berry, and Bernard Girau. (2010). An FPGA design for the stochastic Greenberg-Hastings Cellular Automata. In Waleed Smari, editor, *International Conference on High Performance Computing and Simulation*, pages 565–574, New Jersey, USA. IEEE.

[23] D.J. Watts and S.H. Strogatz. (1998). Collective dynamics of "small-world" networks. *Nature*, 393:440–442.